Available online at www.sciencedirect.com

ScienceDirect

Mendeleev Commun., 2018, **28**, 603–605

Mendeleev Communications

Tuning the surface structure and catalytic performance of $PdIn/Al_2O_3$ in selective liquid-phase hydrogenation by mild oxidative-reductive treatments

Igor S. Mashkovsky,*[a] Nadezhda S. Smirnova,[a] Pavel V. Markov,[a] Galina N. Baeva,[a] Galina O. Bragina,[a] Andrey V. Bukhtiyarov,[b] Igor P. Prosvirin[b] and Aleksandr Yu. Stakheev[a]

[a] *N. D. Zelinsky Institute of Organic Chemistry, Russian Academy of Sciences, 119991 Moscow, Russian Federation. Fax: +7 499 135 5328; e-mail: im@ioc.ac.ru*

[b] *G. K. Boreskov Institute of Catalysis, Siberian Branch of the Russian Academy of Sciences, 630090 Novosibirsk, Russian Federation*

DOI: 10.1016/j.mencom.2018.11.013

The *in situ* DRIFT-CO and XPS data demonstrated that the mild oxidation of PdIn intermetallic nanoparticles results in the partial oxidation of an In component and the transformation of isolated Pd_1 sites to Pd_n multiatomic ones thus enhancing PdIn activity in the liquid-phase hydrogenation of diphenylacetylene without sacrificing the alkene selectivity.

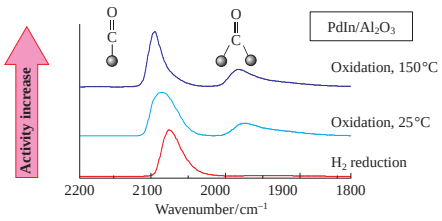

The design and synthesis of active, selective and stable catalysts with uniform active sites is of great importance in modern catalysis.[1] Currently, increasing attention is paid to intermetallic compounds (IMCs) as highly stable and selective heterogeneous catalysts.[2–4] According to a general definition, IMCs are compounds whose crystal structures are different from those of the constituent metals; thus, intermetallic phases and ordered alloys are included.[5] The specific combination of ionic and covalent bonding in IMCs results in the homogeneity of both electronic and crystal structures providing unique catalytic properties. PdZn, PdPb, PdBi, PdFe and PdGa are intensively used IMCs.[2,6–9] Another promising intermetallic composition is PdIn, which was reported as an active catalyst for gas-phase and liquid-phase reactions.[10–14]

A specific surface characteristic of PdGa and PdIn is the isolation of active Pd by Ga or In (the active-site isolation concept, which is similar to the single-atom one).[3,15] This surface structure prevents the formation of di-σ-bonded adsorbed species suppressing undesired reactions and enhances catalyst selectivity and stability.[2,3,16–18] Note that another specific property of PdGa and PdIn IMCs is a high oxophilicity of the Ga or In component. Thus, the formation of oxide phases in the presence of oxygen was observed for PdGa, PdZn, and PdTi IMCs.[4] On the one hand, Ga and In oxophilicity can lead to the instability of IMCs in air, but, on the other hand, it may provide a method of tuning catalytic characteristics by mild and controlled oxidative treatment. To explore this possibility, we investigated the effect of mild oxidation on the surface structure and catalytic performance of $PdIn/Al_2O_3$.

For studying an effect of oxidative treatment, the reduced $PdIn/Al_2O_3$ catalyst was exposed to flowing commercial synthetic air (20 vol% O_2/N_2) at 25 and 150 °C, and its surface structure was investigated by DRIFT-CO and XPS techniques. The catalytic properties of $PdIn/Al_2O_3$ were studied in the liquid-phase hydrogenation of diphenylacetylene (DPA). After oxidation experiments, the catalyst was re-reduced at 250 °C in order to explore the reversibility of changes in the surface structure and catalytic performance caused by oxidation (see Online Supplementary Materials).

The distribution and morphology of PdIn nanoparticles were studied by TEM. A typical micrograph (Figure S1) demonstrates that, after reduction at 500 °C, the $Pd–In/Al_2O_3$ catalyst contained nearly spherical cubo-octahedral nanoparticles surrounded by a less contrast amorphous phase of the support. The particle size distribution is relatively narrow between 2.5 and 6 nm with a maximum at 4.5 nm.

Figure 1 shows the DRIFT spectra of adsorbed CO in the carbonyl region (1800–2200 cm^{-1}) of the bimetallic $Pd–In/Al_2O_3$ sample after different treatments. The absorption band at 2090–2060 cm^{-1} corresponds to linearly adsorbed CO on a palladium surface, whereas the peaks in a range of 2000–1800 cm^{-1} refer to multi-bonded CO. For Pd–In catalyst after *in situ* reduction (see Figure 1, spectrum *1*), an intense absorption band at 2066 cm^{-1}

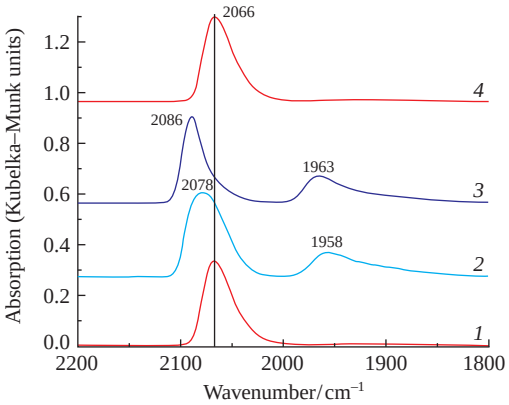

Figure 1 DRIFT-CO spectra for $PdIn/Al_2O_3$ catalyst after the following *in situ* treatments: (*1*) reduction at 500 °C in H_2/Ar, 1.5 h, (*2*) oxidation at 25 °C in O_2/N_2, 30 min, (*3*) oxidation at 150 °C in O_2/N_2, 30 min, and (*4*) reduction at 250 °C in H_2/Ar, 1.5 h. For experimental details, see Online Supplementary Materials.

is observed, which corresponds to the stretching vibrations of CO linearly adsorbed on palladium atoms.[16] Note that the absorption maximum is shifted toward lower frequency relative to the linear CO adsorbed on monometallic Pd/Al_2O_3 (2090 cm^{-1}). The complete absence of bridge-bonded CO indicates the formation of an ordered PdIn intermetallic structure, where indium atoms isolate each Pd atom (Pd_1 centers). The formation of isolated Pd_1 sites is consistent with the previously reported DFT data.[13]

The oxidative treatment of $Pd–In/Al_2O_3$ at 25 °C (see Figure 1, spectrum *2*) leads to a shift of the linear CO band toward higher frequency by ~12 cm^{-1}. The signal of linearly bonded CO becomes broader with a shoulder in the range of lower frequencies. The peak asymmetry indicates the presence of a part of the initial intermetallic PdIn species on the catalyst surface. In addition, the appearance of a broad peak at 2000–1900 cm^{-1} is attributed to the bridge-bonded CO. The following oxidation at 150 °C (see Figure 1, spectrum *3*) leads to more pronounced changes in the surface state. The linear CO band maximum shifts to 2086 cm^{-1}, which is closer to the linear adsorbed CO on a monometallic palladium surface (~2090 cm^{-1}).[16] The band at 2066 cm^{-1} almost completely disappears, while the peak intensity at 1963 cm^{-1} increases. There are no absorption bands with a frequency lower than 1930 cm^{-1}, indicating the absence of hollow-bonded CO.[19] This observation suggests the formation of a new type of active centers presumably consisting of two neighboring palladium atoms (Pd–Pd dimers) on the catalyst surface.[20]

The subsequent reductive treatment at 250 °C for 1.5 h (see Figure 1, spectrum *4*) results in a reverse shift of the linear CO band to 2066 cm^{-1} and the complete disappearance of bridge-bonded CO. These results demonstrate the complete recovery of isolated Pd_1 sites upon mild reduction. The observed changes are consistent with previously reported data on easy transformations of a bimetallic PdIn surface upon different treatments.[16]

The mild oxidation on $PdIn/Al_2O_3$ surface structure was studied by X-ray photoelectron spectroscopy by monitoring the Pd 3*d* and In 2*p* regions (Figure 2, Table 1). For the catalyst reduced at 450 °C, the Pd $3d_{5/2}$ peak is observed at a binding energy of ~335.7 ± 0.1 eV characteristic of Pd^0. Note that the binding energy is higher than the binding energy characteristic of monometallic Pd (334.9 ± 0.1 eV) indicating the formation of PdIn intermetallic compound.[21] The In $3d_{5/2}$ peak is located at 443.6 ± 0.1 eV typical of metallic In.[22] The XPS data also indicate that the In/Pd atomic surface ratio (~1.05) corresponds to the stoichiometry of PdIn intermetallic compound. The data point to the absence of a notable surface enrichment in In or Pd, which is in line with published data on the stability of intermetallic compounds against segregation.[4]

Mild oxidation of the catalyst at 25 °C results in a minor shift of In $3d_{5/2}$ toward higher binding energies by ~0.3 eV. After the oxidation treatment at 150 °C, this shift becomes more pronounced, and the peak maximum is observed at ~444.5 eV indicating the oxidation of In. Simultaneously, the In/Pd atomic ratio gradually increases to 1.40 and 1.60. These observations indicate that the mild oxidation of $PdIn/Al_2O_3$ results in the partial oxidation of an In component causing indium segregation

Table 1 XPS data for the $PdIn/Al_2O_3$ catalyst.

Treatment	Binding energies/eV		In/Pd	In/Al	Pd/Al	(Pd+In)/Al
	Pd $3d_{5/2}$	In $3d_{5/2}$				
H_2, 450 °C, 100 mbar	335.7	443.6	1.05	0.015	0.015	0.034
O_2, 25 °C, 200 mbar	335.7	443.9	1.40	0.021	0.015	0.036
O_2, 150 °C, 200 mbar	335.6	444.5	1.60	0.023	0.014	0.037
H_2, 450 °C, 100 mbar	335.7	443.6	1.01	0.015	0.015	0.034

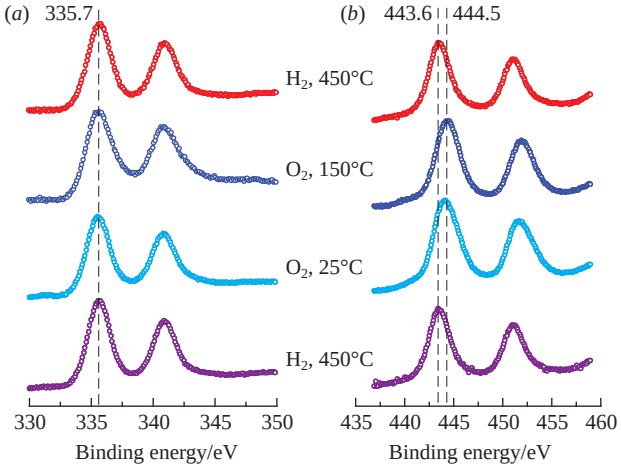

Figure 2 (*a*) Pd 3*d* and (*b*) In 3*d* XPS spectra of $PdIn/Al_2O_3$ catalysts treated under different conditions. For experimental details, see Online Supplementary Materials.

on the surface of PdIn nanoparticles. The oxidative treatments do not affect the position of the Pd $3d_{5/2}$ line (335.7 ± 0.1 eV) indicating that Pd remains in a metallic state. The observed changes in PdIn surface structure caused by indium oxidation/segregation are consistent with the thermodynamic data: $\Delta G_f(In_2O_3)$ = = –926.4 kJ mol^{-1}, while $\Delta G_f(PdO)$ = –115.6 kJ mol^{-1}.[23]

By comparing the XPS and DRIFT-CO data, we can conclude that the oxidative treatments significantly affect the surface structure of PdIn nanoparticles. Because of high oxophilicity, the In component is selectively oxidized, presumably forming InO_x surface species. This results in the deterioration of Pd_1 site isolation and the formation of Pdn multiatomic sites, as indicated by the appearance of a bridge-bonded CO peak in DRIFT-CO spectra. It is important that the Pd site-isolated structure can be easily recovered even by reduction at 250 °C. Such a treatment results in In reduction, which is accompanied by a decrease in the surface In/Pd ratio to a value characteristic of the intermetallic PdIn surface (~1.01). The disappearance of the bridge-bonded CO peak and the shift of the linear adsorbed CO peak to 2066 cm^{-1} in DRIFT-CO spectra (see Figure 1, spectrum *4*) evidence the restoration of isolated Pd_1 sites.

The effect of $PdIn/Al_2O_3$ oxidation/reduction on the performance in DPA hydrogenation is shown in Figure S2 (see Online Supplementary Materials) by comparing H_2 uptake profiles for the reduced catalyst and the catalyst subjected to oxidative treatments at 25 and 150 °C. Table 2 summarizes the rates of hydrogen uptake at the stages of alkyne (r_1) and alkene (r_2) hydrogenation, turnover frequencies at both stages, and selectivity for diphenylethylene (DPE) on the reduced and oxidized catalysts.

Analyzing the kinetic profiles of H_2 uptake and TOF values for the reduced $PdIn/Al_2O_3$ and the catalyst after oxidative treatment, we can conclude that oxidation significantly increases the rate of hydrogenation. Thus, turnover frequency in alkyne hydrogenation (TOF_1) increases twofold after oxidation at room temperature from 0.018 to 0.044 s^{-1} and almost by an order of magnitude (to 0.17 s^{-1}) after oxidation at 150 °C.

The observed activity enhancement presumably stems from the transformation of isolated Pd_1 to multiatomic Pd_n centers (presumably dimeric Pd_2 sites, as evidenced by DRIFT-CO). This observation is in line with the previously reported results,[20] indicating that the presence of the Pd–Pd dimers on the surface of PdCu clusters enhanced activity in acetylene hydrogenation. A possible explanation of the activity enhancement was confirmed by DFT calculations, which demonstrated that Pd clusters in the surface and sub-surface regions of PdCu are more effective sites for H_2 dissociation than isolated Pd_1 centers.[24]

Table 2 Kinetic parameters of liquid-phase alkyne hydrogenation and selectivity for DPE formation at P_{H_2} = 5 bar and T = 25 °C.[a]

Treatment	r_1/mmol min^{-1} g_{cat}^{-1}	r_2/mmol min^{-1} g_{cat}^{-1}	TOF_1/s^{-1}	TOF_2/s^{-1}	TOF_1/TOF_2	S_{cis} (%)[b]	S_{trans} (%)[b]	$S_=$ (%)[c]	
								$X_{50\%}$ (%)	$X_{95\%}$ (%)
H_2, 500 °C	0.25	0.007	0.018	0.0005	36.0	95.4	4.6	97.0	96.0
O_2/N_2, 25 °C, 30 min	0.62	0.015	0.044	0.0011	40.7	94.7	4.3	96.8	95.3
O_2/N_2, 150 °C, 30 min	2.38	0.121	0.169	0.0086	19.6	93.5	4.5	96.7	94.3
H_2, 250 °C	0.26	0.007	0.019	0.0005	38.0	95.6	4.4	97.1	95.9

[a] See ref. 25 for details of calculations. [b] Selectivity was determined at DPA conversions of 95% ($X_{95\%}$). [c] Selectivity was determined at DPA conversions of 50% ($X_{50\%}$) and 95% ($X_{95\%}$).

Remarkably, $PdIn/Al_2O_3$ retains high selectivity in alkene formation after oxidation at 150 °C (see Table 2) despite the transformation of isolated Pd_1 sites to multiatomic Pd_n surface centers upon oxidative treatment. This observation suggests that the high selectivity of $PdIn/Al_2O_3$ is due to the hindering of subsurface hydride formation (since PdIn is not capable to adsorb hydrogen[18]) rather than site isolation of Pd_1 centers.

It is important that the subsequent reduction at 250 °C completely restores the catalytic characteristics of $PdIn/Al_2O_3$ (see Table 2), which is in agreement with CO-FTIR and XPS data.

Thus, a comparison of the characterization data and the catalytic results for $PdIn/Al_2O_3$ demonstrate that the mild oxidative treatment makes it possible to tune the structure of active sites on the surface of Pd nanoparticles. Partial oxidation of indium component deteriorates the isolation of Pd sites and leads to the transformation of a part of isolated Pd sites to multiatomic Pd_n centers demonstrating high hydrogenation activity.

This study was supported by the Russian Science Foundation (grant no. 16-13-10530). The catalyst characterization by electron microscopy was performed at the Department of Structural Studies of the N. D. Zelinsky Institute of Organic Chemistry, Russian Academy of Sciences. We are grateful to Professor M. N. Vargaftik and Dr. I. A. Yakushev (N. S. Kurnakov Institute of General and Inorganic Chemistry, Russian Academy of Sciences) for supplying us with the $Pd(\mu\text{-}O_2CMe)_4In(O_2CMe)$ complex, which was used as a precursor for the catalyst preparation.

Online Supplementary Materials

Supplementary data associated with this article can be found in the online version at doi: 10.1016/j.mencom.2018.11.013.

References

1 V. P. Ananikov, D. B. Eremin, S. A. Yakukhnov, A. D. Dilman, V. V. Levin, M. P. Egorov, S. S. Karlov, L. M. Kustov, A. L. Tarasov, A. A. Greish, A. A. Shesterkina, A. M. Sakharov, Z. N. Nysenko, A. B. Sheremetev, A. Yu. Stakheev, I. S. Mashkovsky, A. Yu. Sukhorukov, S. L. Ioffe, A. O. Terent'ev, V. A. Vil', Yu. V. Tomilov, R. A. Novikov, S. G. Zlotin, A. S. Kucherenko, N. E. Ustyuzhanina, V. B. Krylov, Yu. E. Tsvetkov, M. L. Gening and N. E. Nifantiev, *Mendeleev Commun.*, 2017, **27**, 425.

2 M. Armbrüster, M. Behrens, F. Cinquini, K. Föttinger, Y. Grin, A. Haghofer, B. Klötzer, A. Knop-Gericke, H. Lorenz, A. Ota, S. Penner, J. Prinz, C. Rameshan, Z. Révay, D. Rosenthal, G. Rupprechter, P. Sautet, R. Schlögl, L. Shao, L. Szentmiklósi, D. Teschner, D. Torres, R. Wagner, R. Widmer and G.Wowsnick, *ChemCatChem*, 2012, **4**, 1048.

3 M. Krajči and J. Hafner, *ChemCatChem*, 2016, **8**, 34.

4 S. Furukawa and T. Komatsu, *ACS Catal.*, 2017, **7**, 735.

5 G. Sauthoff, *Intermetallics*, Wiley-VCH, Weinheim, 1995.

6 M. Armbrüster, M. Behrens, K. Föttinger, M. Friedrich, É. Gaudry, S. K. Matam and H. R. Sharma, *Catal. Rev. Sci. Eng.*, 2013, **55**, 289.

7 K. Föttinger, *Catalysis*, 2013, **25**, 77.

8 S. Furukawa and T. Komatsu, *ACS Catal.*, 2016, **6**, 2121.

9 S. Furukawa, M. Endo and T. Komatsu, *ACS Catal.*, 2014, **4**, 3533.

10 M. Neumann, D. Teschner, A. Knop-Gericke, W. Reschetilowski and M. Armbrüster, *J. Catal.*, 2016, **340**, 49.

11 H. Lorenz, S. Turner, O. I. Lebedev, G. Van Tendeloo, B. Klötzer, C. Rameshan, K. Pfaller and S. Penner, *Appl. Catal. A*, 2010, **374**, 180.

12 Y. Cao, Z. Sui, Y. Zhu, X. Zhou and D. Chen, *ACS Catal.*, 2017, **7**, 7835.

13 Q. Feng, S. Zhao, Y. Wang, J. Dong, W. Chen, D. He, D. Wang, J. Yang, Y. Zhu, H. Zhu, L. Gu, Z. Li, Y. Liu, R. Yu, J. Li and Y. Li, *J. Am. Chem. Soc.*, 2017, **139**, 7294.

14 A. García-Trenco, A. Regoutz, E. R. White, D. J. Payne, M. S. P. Shaffer and C. K. Williams, *Appl. Catal. B*, 2018, **220**, 9.

15 X.-F. Yang, A. Wang, B. Qiao, J. Li, J. Liu and T. Zhang, *Acc. Chem. Res.*, 2013, **46**, 1740.

16 A. Yu. Stakheev, N. S. Smirnova, D. S. Krivoruchenko, G. N. Baeva, I. S. Mashkovsky, I. A. Yakushev and M. N. Vargaftik, *Mendeleev Commun.*, 2017, **27**, 515.

17 P. V. Markov, G. O. Bragina, A. V. Rassolov, I. S. Mashkovsky, G. N. Baeva, O. P. Tkachenko, I. A. Yakushev, M. N. Vargaftik and A. Yu. Stakheev, *Mendeleev Commun.*, 2016, **26**, 494.

18 M. Wencka, M. Hahne, A. Kocjan, S. Vrtnik, P. Koželj, D. Korže, Z. Jagličić, M. Sorić, P. Popčević, J. Ivkov, A. Smontara, P. Gille, S. Jurga, P. Tomeš, S. Paschen, A. Ormeci, M. Armbrüster, Yu. Grin and J. Dolinšek, *Intermetallics*, 2014, **55**, 56.

19 T. Lear, R. Marshall, J. A. Lopez-Sanchez, S. D. Jackson, T. M. Klapotke, M. Baumer, G. Rupprechter, H.-J. Freund and D. Lennon, *J. Chem. Phys.*, 2005, **123**, 174706.

20 A. J. McCue and J. A. Anderson, *J. Catal.*, 2015, **329**, 538.

21 C. Rameshan, H. Lorenz, L. Mayr, S. Penner, D. Zemlyanov, R. Arrigo, M. Haevecker, R. Blume, A. Knop-Gericke, R. Schlögl and B. Klötzer, *J. Catal.*, 2012, **295**, 186.

22 I. A. Witońska, M. J. Walock, P. Dziugan, S. Karski and A. V. Stanishevsky, *Appl. Surf. Sci.*, 2013, **273**, 330.

23 É. Gaudry, G. M. McGuirk, J. Ledieu and V. Fournée, *J. Chem. Phys.*, 2014, **141**, 084703.

24 Q. Fu and Y. Luo, *ACS Catal.*, 2013, **3**, 1245.

25 P. V. Markov, G. O. Bragina, A. V. Rassolov, G. N. Baeva, I. S. Mashkovsky, V. Yu. Murzin, Ya. V. Zubavichus and A. Yu. Stakheev, *Mendeleev Commun.*, 2016, **26**, 502.

Received: 6th July 2018; Com. 18/5644